External Morphology and Internal Zonal Structure of Macle Diamond

Ahmadjan Abduriyim and Masao Kitamura

Contact-twinned crystals of natural diamond rough, known as "macle," typically exhibit a flattened triangular shape, which has been attributed to preferential growth at re-entrant corners where two crystals mutually contact. The influence of the re-entrant corner effect on the morphological alteration of macle diamond may be closely linked to the conditions of carbon supersaturation. However, no detailed investigation has been conducted regarding the possibility of preferential growth on the opposite side of the re-entrant corner, which is referred to as a "salient corner" in this study. The four external and internal growth morphologies (I, II, III, and IV) of contact-twinned macle diamonds with four different corresponding re-entrant corner shapes (i, ii, iii, and iv) were analyzed by examining the surface features of each corner and the zonal growth structure through scanning electron microscopy–cathodoluminescence images. The study confirmed that morphological changes and the flatness of macle diamonds resulted from preferential growth at both re-entrant and salient corners. To our knowledge, this is the first reporting of group III and IV macle crystals characterized by an apex covered by high-index {hhk} faces as well as the salient corner effect. Additionally, the variations in morphology appear to correlate with fluctuations in carbon supersaturation conditions in the diamonds' growth medium.

The most distinctive type of contact-twinned crystals are the triangular *macle* (French for "twin") diamonds (figure 1). These diamonds consist of two octahedral crystals in contact with each other on the (111) octahedral face, with the twin plane parallel to the octahedral <111> direction. These crystals often grow significantly larger than the sum of the two single octahedral diamond crystals would be, displaying the characteristic morphology of a flattened triangular shape (Sinkankas, 1964; Orlov, 1977; Tappert and Tappert, 2011). Due to dissolution, macle diamonds may also lose their sharp edges and develop a rounded habit. In some South African diamond mines, an average of 10–15% of diamonds are macle crystals (Harris et al., 1975). Twinning also occurs in synthetic diamonds grown by chemical vapor deposition (CVD), with the contact twin mechanism originating from the formation of a hydrogen-terminated four-carbon atom cluster on the {111} surface during polycrystalline diamond growth (Battaile et al., 1998; Butler and Oleynik, 2008).

See end of article for About the Authors and Acknowledgments.
Gems & Gemology, Vol. 61, No. 3, pp. 250–269,
http://dx.doi.org/10.5741/GEMS.61.3.250

The crystal faces {111} are crystallographically equivalent in single octahedral diamonds (figure 2, A and B), and there is no difference in the growth rates of these {111} faces. Additionally, there is no change in growth morphology under stable growth conditions (Hartman, 1956). Therefore, estimating changes in growth conditions is quite challenging. However, in the case of contact-twinned crystals, the growth rates of the {111} faces are not equivalent.

In Brief

- "Macle" refers to a twinned diamond with a flat triangular shape, formed when two single diamonds contact each other during the growth process.
- Morphologies of macle diamonds with different re-entrant corner shapes are classified into distinct morphology groups (I, II, III, and IV) with corresponding re-entrant corner shapes (i, ii, iii, and iv). These morphologies are explained by preferential growth effects at the corners.
- The flatness and changes in the morphology of macle diamonds are directly related to preferential growth occurring at the re-entrant and salient corners under different carbon supersaturation conditions.

Figure 1. Examples of contact-twinned macle diamond crystals from South Africa. Left to right: a flat triangular macle with limited resorption (sample 11; 0.357 ct); an extensively resorbed variant of a flat triangular macle (sample 12; 0.411 ct); a very elongated flat macle with stacking growth layers on the octahedral faces, showcasing sharp edges and pointed apex corners (sample 13; 0.553 ct); a six-pointed star-shaped, poorly resorbed flat macle (sample 14; 0.747 ct). Photo by Tetsuya Chikayama; courtesy of Suwa & Son, Inc.

The octahedral {111} faces are categorized into three types depending on their relation to the twin boundary (junction): (1) faces *r* and *r**, which are not parallel to the twin plane and form re-entrant corners with an interfacial angle of 141.06°; (2) faces *s* and *s**, which are not parallel to the twin plane and form salient corners with an interfacial angle of 218.94° (figure 2D); and (3) faces *n* and *n**, which do not contact re-entrant and salient corners and are parallel to the twin plane.

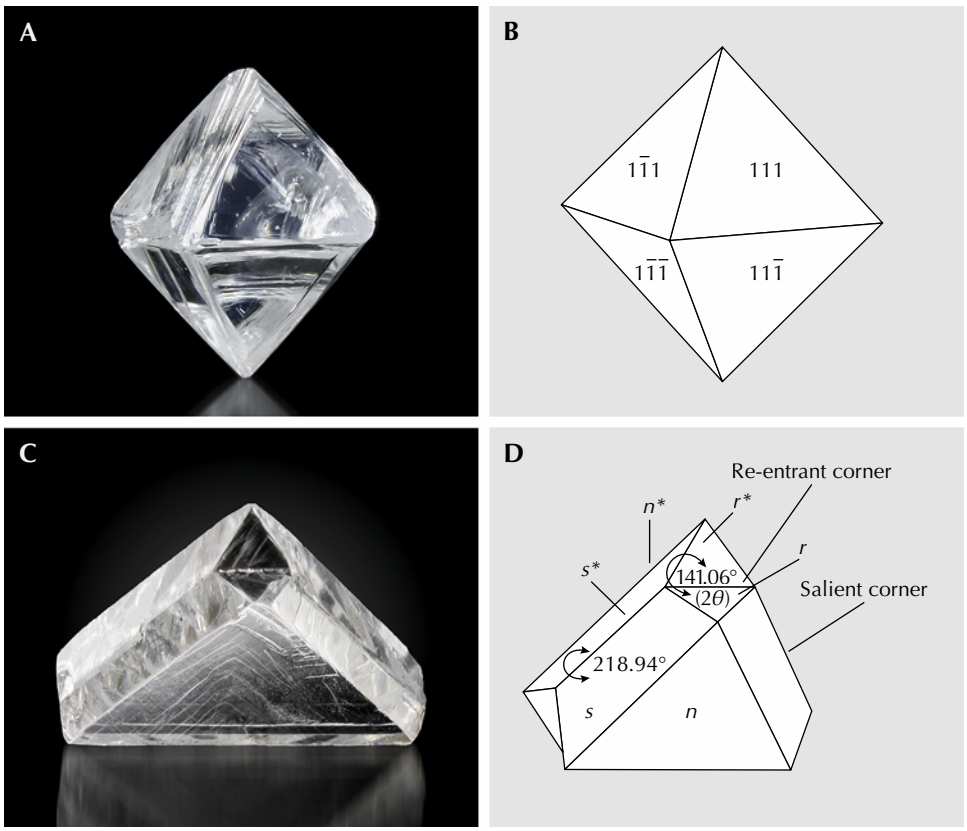

*Figure 2. A: A natural single octahedral crystal diamond bounded by {111} faces (3.51 × 3.50 × 6.18 mm). B: Illustration of an octahedral diamond. All of the {111} faces are crystallographically equivalent. C: A contact-twinned macle diamond, characterized by its {111} faces (7.74 × 7.63 × 2.86 mm). D: Illustration of a contact twin. The {111} faces are categorized into three types (*r *and* r*, s *and* s*, *and* n *and* n*) *according to their relationship with the twin boundary. Photos by Tetsuya Chikayama; courtesy of Suwa & Son, Inc. (C).*

The characteristic morphology of twinned crystals has been studied based on the re-entrant corner effect resulting from preferential nucleation at the corner (Becke, 1911; Chudoba, 1927; Stranski, 1949; Hartman, 1956), as well as the "pseudo-re-entrant corner" effect attributed to the concentration of screw dislocations on the twin boundary at the corner. These studies aim to explain the distinctive morphologies of twinned crystals (Kitamura et al., 1979). The preferential growth at the re-entrant corners has also been emphasized to elucidate the flattened morphology of contact-twinned crystals, including the parallel axes of contact-twinned spinel and macle diamond, the inclined axes of heart-shaped Japan law–twinned quartz, the V-shaped twin of amethyst, the V-shaped twin of rutile, the swallowtail-shaped twin of gypsum, the butterfly-shaped twin of calcite, and the Brazil law twin of hematite (figure 3) (Sunagawa, 1975; Sunagawa et al., 1979; Sunagawa and Yasuda, 1983; Sunagawa and Lu, 1987; Ming and Sunagawa, 1988; Kitamura et al., 1992; Hirabayashi et al., 1993). However, to our knowledge, no detailed study has been conducted on the potential for preferential growth at the salient corners of macle diamond crystals.

In this study, the authors aim to introduce a model that facilitates understanding of the morphological changes of contact twins based on the growth rates of octahedral faces {111} *r* and *r** at the re-entrant corners, *s* and *s** at the salient corners, and *n* and *n** that do not interact with these corners. Specifically, the study presents detailed results regarding the morphological changes of macle diamonds during the growth process by exploring their three-dimensional internal zonal structure, which chronicles the morphological changes during crystal formation and estimates the growth rate ratios based on growth zoning. The fluctuation in carbon supersaturation conditions during crystallization can be influenced by the addition of a carbon source to the growth system or a significant change in pressure and temperature conditions. The increase or decrease in carbon supersaturation conditions is also estimated in this study based on the observed morphological changes.

MATERIALS AND METHODS

Samples. Fourteen selected rough macle diamonds from South Africa (samples 1–14) were used in this study. The crystals ranged in weight from 0.118 to 0.747 ct, with one side length varying from 2.4 to 6.3 mm and colors spanning from colorless to light yellow and very light pink. Samples 1–10 were provided by the Department of Geology and Mineralogy at Kyoto University. Samples 11–14 were loaned by Suwa & Son, Inc. and were used only to study the external morphology.

Microscopic Observation. The external morphology and surface microtopography of these macle diamonds were examined using an Olympus SZX optical microscope equipped with a 0.8× objective lens and an Olympus BX51 differential interference contrast microscope (DICM). Photographs were taken using a Nikon DS-Ri2 camera.

Scanning Electron Microscopy–Cathodoluminescence (SEM-CL). To investigate the internal zonal structure and morphological changes during the growth process, four samples (1, 3, 6, and 10) were prepared for SEM-CL observation. These four crystals were sliced with a diamond saw (ref 1002, Bettonshop Israel Ltd.) in one direction through the center of the re-entrant corner, perpendicular to the twinning plane and parallel to a (110) plane. The cut surfaces were polished using a diamond polishing machine (Imahashi FAC-8) and carbon coated in a vacuum evaporation process. The polished surfaces were subsequently examined under a scanning electron microscope with cathodoluminescence mode (Kitamura et al., 1992; Ponahlo, 1992). The polishing and SEM-CL observation processes were repeated to achieve a surface cut through the crystal's growth center.

Measurement of Growth Band Widths. Based on the zonal structure appearance of the polished surfaces of the four samples, schematic drawings of the growth bands were carefully sketched from the CL image of each crystal; then the growth band widths of each {111} face (*r*, *n*, *s* at the left side and *r**, *n**, *s** at the right side of the twin) were measured. Because the first growth region in the core area of the twin showed a very complex zonal structure and the last growth region at the rim area showed a dissolved curved band, only the mantle region (between the rim and central core) was measured in detail in order to obtain reliable data in this study.

RESULTS

Classification of Re-Entrant Corners and External Morphology of Macle Diamonds. All the macle diamond crystals studied exhibit a flattened triangular morphology with either concave or convex

Figure 3. Representative shapes of contact-twinned flat triangular spinel (0.244–3.422 ct), heart-shaped Japan law–twinned quartz (16.212 ct), V-shaped Japan law–twinned amethyst (69.603 ct), V-shaped contact-twinned rutile (5.176 ct), swallowtail-shaped contact-twinned gypsum (314.02 ct), butterfly-shaped contact-twinned calcite (117.55 ct), and heart-shaped contact-twinned hematite (298.81 ct). Photos by Tetsuya Chikayama.

(apex) shapes at the re-entrant corners (figure 4). Among them, various forms depend on the degree of flatness and types of re-entrant corners. Except for the extremely rounded corners and edges of samples 12 and 13, the other crystals display nearly flat octahedral faces with straight, sharp corners and edges. This suggests that these crystals underwent limited dissolution, indicating that they nearly retained their original as-grown forms (again, see figure 1). Sample 14 resembles a six-pointed star, known as the "Star of David twin," which presents an intergrowth of two macle crystals oriented in opposite directions, featuring well-formed re-entrant and salient surface corners (again, see figure 1).

The morphologies of macle diamond crystals are determined by the four different shapes of the re-entrant corners (i, ii, iii, and iv). These macle morphologies are primarily characterized by growth layers generated at the twin boundaries of the re-entrant corners, and fall into four groups: I, II, III, and IV (figure 5, top).

- Group I morphology consists of nearly flat {111} surfaces and features a concave shape at the re-entrant corners (figure 5, bottom). Samples 1 and 2 (figure 4, A and B) and sample 11 (figure 1) exhibit this re-entrant corner shape (i).
- Group II morphology has a concave re-entrant corner and is defined by two {111} surfaces stacked with a few lamellae growth layers formed at the twin boundary of the re-entrant corners (shape ii). This group includes samples 3 and 4 (figure 4, C and D).
- Group III morphology is characterized by the stacking of thick growth layers formed at the twin boundary, which leads to the formation of four high-index {hhk} faces surrounding a small

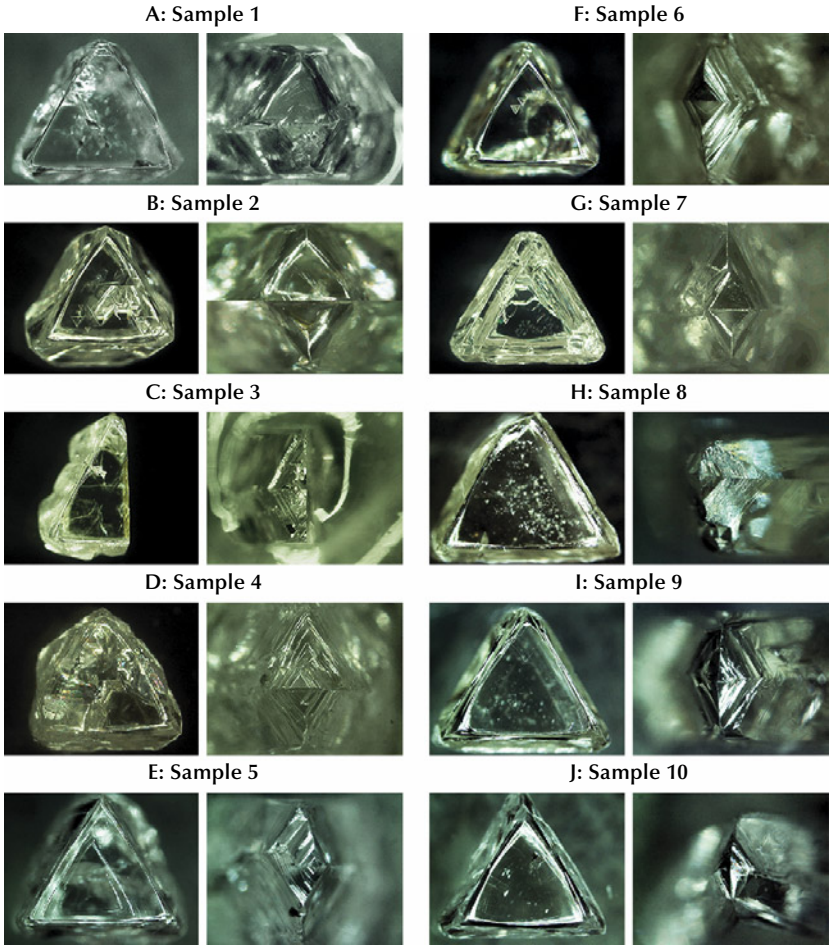

Figure 4. Outlines and distinct shapes of re-entrant corners from macle samples 1–10, with weights ranging from 0.118 to 0.185 ct, sourced from South Africa. Photos by Ahmadjan Abduriyim. Fields of view for the right images of each sample: 2.63 (A), 1.93 (B), 2.49 (C), 2.04 (D), 1.32 (E), 1.67 (F), 1.56 (G), 1.70 (H), 1.70 (I), and 2.10 (J) mm.

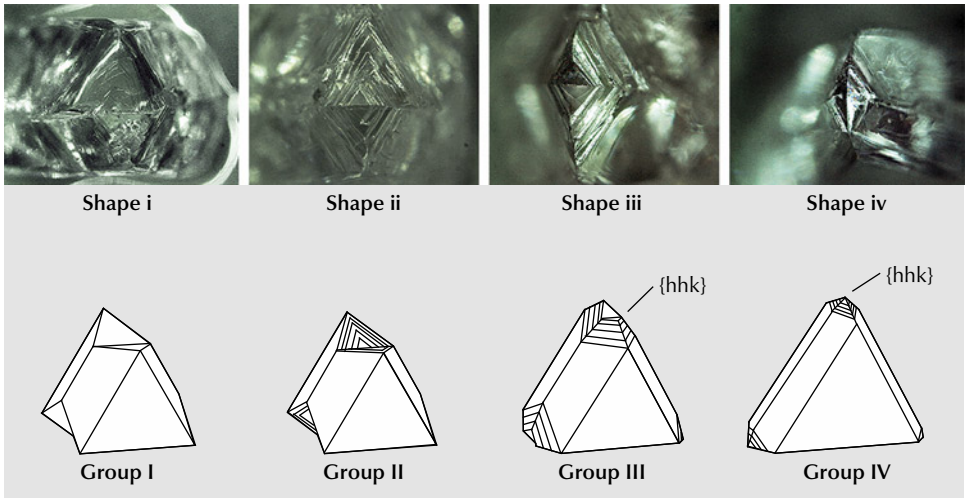

Figure 5. The four re-entrant corner shapes (i, ii, iii, and iv) and illustrations of the external morphologies (I, II, III, and IV) of macle crystals. Photomicrographs by Ahmadjan Abduriyim; fields of view 2.67 mm, 2.40 mm, 1.76 mm, and 2.22 mm, respectively.

concave re-entrant corner (shape iii). This group includes samples 5–7 (figure 4, E–G).

- Group IV morphology is marked by a convex (apex) corner formed by smooth curved surfaces or stepped surfaces, made up entirely of a stack of growth layers at the re-entrant corners (shape iv). This group comprises six crystals: samples 8–10 (figure 4, H–J) and samples 12–14 (figure 1).

External Morphology and Flatness. Samples 1 and 2 exhibit a flattened triangular form with three re-entrant corners, referred to as morphology group I (figure 4, A and B). They have relatively flat {111} faces with slightly rounded corners and edges at the re-entrant corners, along with some growth layers forming on the *s* (*s**) and *n* (*n**) faces. At a prominent corner, the growth layers on the face *s* can be seen protruding to the opposite side. The degree of flatness is 1, based on equation A-1 (see box A).

Samples 3 and 4 display nearly pointed corners and straight edges, but the *r* and *r** surfaces are covered by a few stacking lamellae growth layers at the re-entrant corners, as illustrated in morphology group II (figure 4, C and D). A few developed growth hillocks were observed on the *s* (*s**) and *n* (*n**) surfaces. The degree of flatness is 1.1.

Sample 5 has nearly pointed corners and straight edges, showcasing a flattened triangular shape with three small re-entrant corners, as seen in morphology group III (figure 4E). The growth layers on both {111} faces at the re-entrant corners extend outward from the twin boundaries. During the growth process, the re-entrant corners tend to fill with growth layers, resulting in an apex corner that features four high-index {hhk} faces. Well-developed growth layers are also present on the *s* (*s**) and *n* (*n**) surfaces. The degree of flatness is 1.4. Samples 6 and 7 also belong to the shape III group but have slightly rounded corners and edges and consist of four high-index {hhk} faces with stepped surfaces at the re-entrant corners (figure 4, F and G). Their morphology is significantly flatter than that of sample 5, and the degree of flatness for both crystals is 2.2.

Sample 8 has re-entrant corners fully covered by four high-index {hhk} faces with stepped lamellae growth layers, forming three apexes instead of re-entrant corners, resembling morphology group IV (figure 4H). At the salient corners, well-developed growth layers were observed around the twin boundary (plane). The degree of flatness is 2.4. Samples 9 and 10 also belong to the shape IV group, and the four high-index {hhk} faces exhibit a very smooth curved surface feature (figure 4, I and J). The development of growth layers around the twin boundary at the salient corner was noted. The degree of flatness for both crystals is 3.3.

These results indicate that the value of the flatness indicator (equation A-1; see box A) increases as the flatness of contact-twinned macle diamonds increases.

Surface Microtopography. The surface microtopography of octahedral faces varies significantly from crystal to crystal and even from face to face on a single crystal. The 12 octahedral {111} faces (6 faces at the re-entrant corners and 6 faces at the salient corners) of most samples exhibit mirror-smooth, uniform surfaces and sharp edges characterized by stacked triangular growth layer lamellae of progressively diminishing size. Some faces display a pronounced blocky stepped growth structure. These mirror-smooth growth layers and sharp stepped

BOX A: MEASUREMENT OF MACLE DIAMOND FLATNESS

To indicate the flatness of contact-twinned crystals, the ratio of the sum of the height of a triangular octahedral face (h) and the height of an edge of the apex corner (h') to the thickness (d) of the crystal is defined as the flatness indicator (f) of external morphology (as illustrated in figure A-1):

$$f = \frac{(h+h')}{d} \qquad \text{(A-1)}$$

When two regular octahedral crystals contact each other, the calculated degree of flatness is $3\sqrt{2}/8$. In contrast to this ideal morphology, the heights of the n face (h), the edge of the apex corner (h'), and the thickness (d) of samples 1–10 were measured. (Note: Samples 11–14 were not measured for their flatness.)

*Figure A-1. Macle crystals with ideal morphology illustrating how to measure the flatness of the contact-twinned crystals. The flatness indicator variables (*h, h', l, d*), and the* θ *and* α *angles are labeled, where* h *is the height of the triangular octahedral face;* h' *is the height of the apex corner edge;* l *is the length of the apex corner edge;* d *is macle thickness;* θ *is the internal angle between the twin plane and face* r*; and* α *is the internal angle between the re-entrant corner edge and face* n.

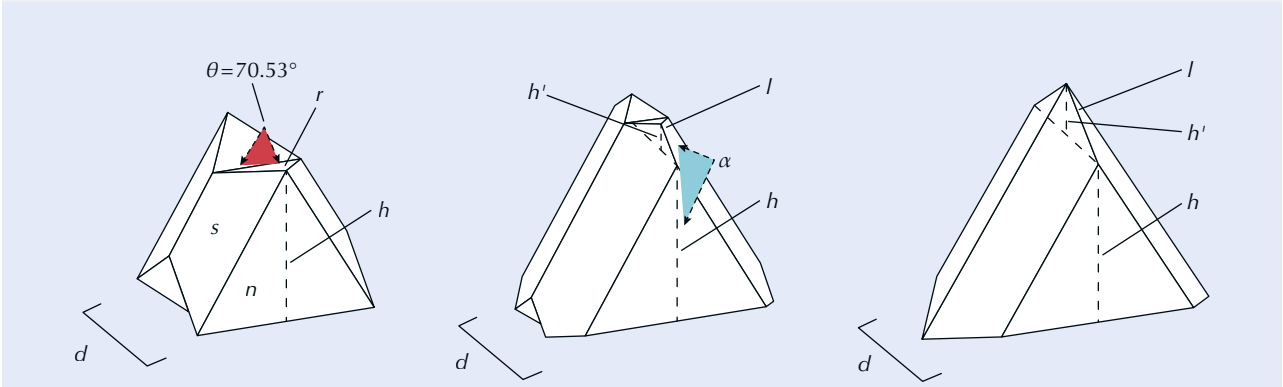

growth structures retain nearly all original as-grown features. The corners and edges of a few samples exhibit slightly rounded forms, with curved faces and deep etch pits known as trigons on their surfaces, indicating that these crystals underwent mild dissolution. Based on the analysis of microtopography, the characteristic morphologies of growth layers on the octahedral faces can be categorized into two types, depending on the generation of growth layers around twin boundaries or on the surfaces of the octahedral faces. The first type consists of spiral-stepped stacked lamellae growth layers that develop at the center of small r faces and large n faces, alongside polycentric stacked lamellae growth layers on the trapezoid-shaped s faces (figure 6). The second type involves the formation of single large mirror-smooth growth layers on the large n faces, stacked lamellae growth layers on the small r faces around the twin boundary of the re-entrant corners, and several thick stepped block growth layers on the trapezoid-shaped s faces near the twin boundary of the salient corners (figure 7). As a result of the observations of the microtopography surface structure, the surfaces r and r^* at the three re-entrant corners and the surfaces s and s^* at the three salient corners of the morphology group I and II macle crystals demonstrate very smooth, flat growth layers. Compared to morphology groups I and II, group III reveals two types of growth layer structures: one involves thick lamellae growth layers developing or originating from the twin boundary at the re-entrant and salient corners, while the other features spiral-stepped growth layers forming at the center of r and r^* and s and s^* surfaces. In morphology group IV, the growth layer structure of faces r and r^* at the re-entrant corner is unobservable, as it has been replaced by an apex corner, with very thick blocky lamellae layers emerging from the twin boundary at the salient corner being predominant.

Distribution of Trigons. The octahedral faces almost invariably display triangular depressions (trigons) that are oriented opposite the triangles of the octahedral faces. These trigons arise from dissolution (Frank et al., 1958), primarily at dislocation outcrops

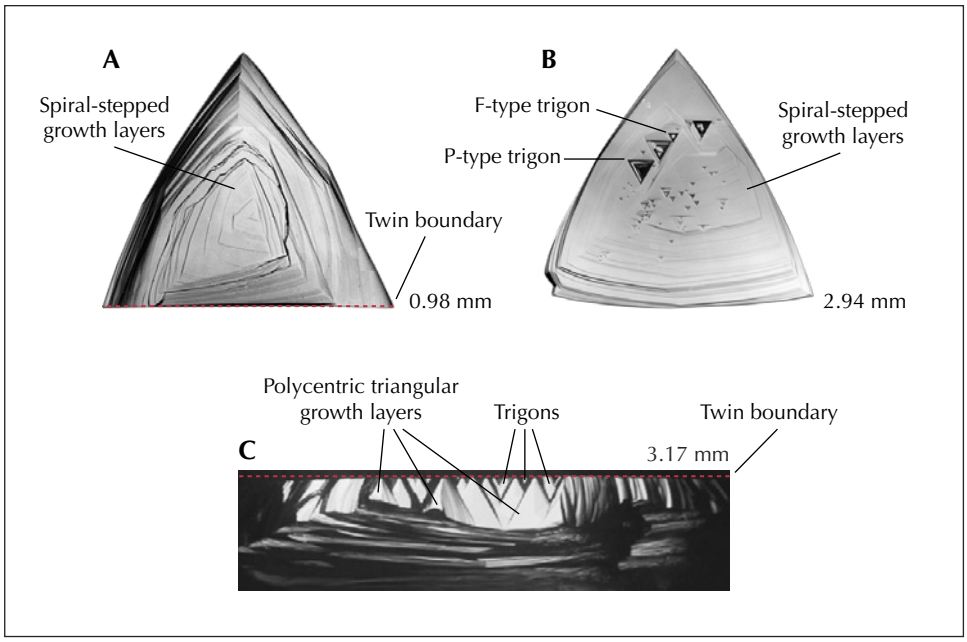

Figure 6. A: The micro-surface structure of a contact-twinned macle diamond features well-developed stacked triangular spiral-stepped laminae growth layers on an r *face. B: The spiral-stepped (shield-shaped) laminae growth layers are generated on face* n*. The features of the P-type (pointed bottom) trigon and F-type (flat bottom) trigon are preserved on this surface. C: Face* s *displays a distinct poly-centric development of small triangular stacked growth layers. Photos by Ahmadjan Abduriyim.*

(Lang, 1964). There is a one-to-one correlation between screw-type dislocation outcrops and the centers of growth layers (Sunagawa et al., 1984). This shows that natural diamonds' stacked lamellae growth layers develop through a spiral growth mechanism under low supersaturation conditions. Consequently, the well-defined growth layers on the octahedral faces or twin boundaries are affected by the density of screw dislocations protruding from the surfaces.

Trigons were noted on most octahedral faces and twin boundaries, although this does not necessarily mean that all octahedral faces have trigons. The number of trigons on a single face varies between crystals and from face to face. The two primary types of trigons are pointed-bottomed (P-type) and flat-bottomed (F-type).

Trigon density was assessed on all octahedral faces and at the twin boundaries of samples 1 (morphology group I), 3 (morphology group II),

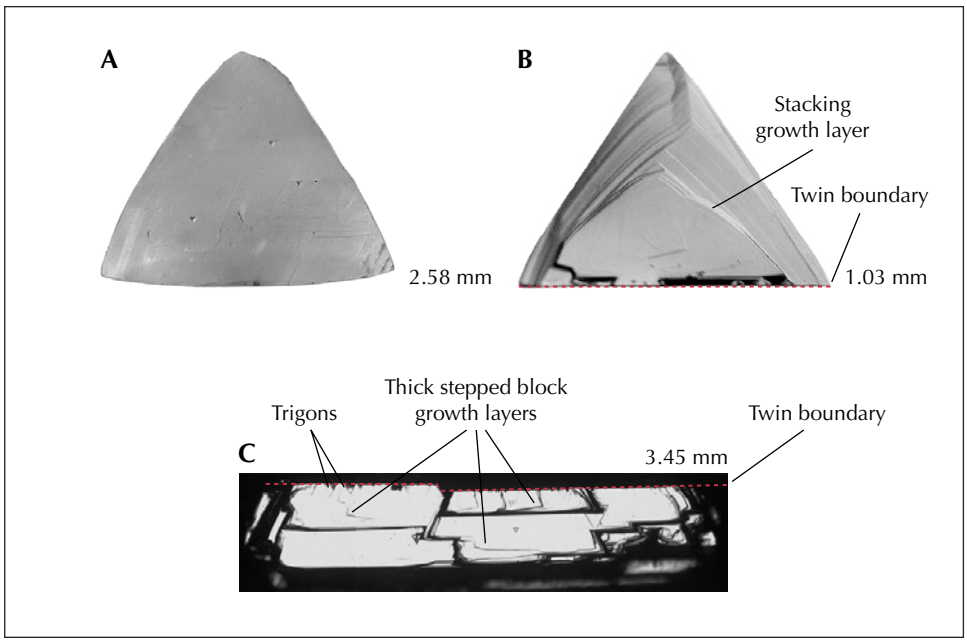

Figure 7. A: The micro-surface structure of face n *is characterized by a featureless (or mirror-like) surface. B: Triangular stacking lamellae growth layers on face* r *originated from the twin boundary at the re-entrant corner. C: Thick stepped block growth layers originated from the twin boundary at the salient corner. Photos by Ahmadjan Abduriyim.*

6 (morphology group III), and 10 (morphology group IV). The number of trigons on one face differs from locality to locality within a face and from face to face. The number of trigons observed on the surfaces and at the twin boundaries of each group, along with the density of trigons per unit area (number/mm^2), is illustrated in figure 8.

The data from samples 1 to 10 clearly reveal an increase in the number and density of trigons at the *s* and *s** face of salient corners and the twin boundaries. Sample 1 exhibits a higher density of trigons at the *r* and *r** surface and twin boundaries than at the *s* and *s** surface. The trigon density at each face of re-entrant and salient corners and twin boundaries shows an increasing trend from samples 4 to 6. For sample 10, we could not account for the trigons at the re-entrant corners due to coverage by high-index {hhk} faces. The density of trigons at the *s* and *s** faces gradually increases from samples 1 to 10, with the highest density noted at the *n* and *n** faces.

For morphology group I, surface microtopographical features such as growth layers and trigons do not significantly appear on salient corners; therefore, a highly flattened morphology cannot be anticipated. In contrast, the macle diamonds in morphology group IV demonstrate a markedly higher density than those in the other groups. This suggests that preferential growth can be expected from the screw dislocations on such surfaces, and the flatness is much more pronounced.

Internal Zonal Structure and Morphological Changes of Macle Diamonds During Growth. Natural diamonds are known to exhibit a well-defined zonal structure during their crystallization process. This growth zoning provides significant insights into the morphological changes in crystals, revealing their growth history. Several studies have clarified contact-twinned diamond crystals' internal structure and growth history (Kitamura, 1990; Yacoot et al., 1998; Abduriyim and Kitamura, 2002). The following subsections individually describe the zonal structures of four crystals from four morphology groups defined in this paper.

Observation of Internal Zonal Structure. Mosaic photographs of CL images show two successive polished surfaces sliced on the (110) plane of sample 1. One of the sliced planes is believed to be the center of the macle crystal, as illustrated in figure 9A, with a detailed schematic drawing based on the zonal structure observed in the CL image. This zonal structure features oscillatory zones characterized by alternating light and dark growth bands.

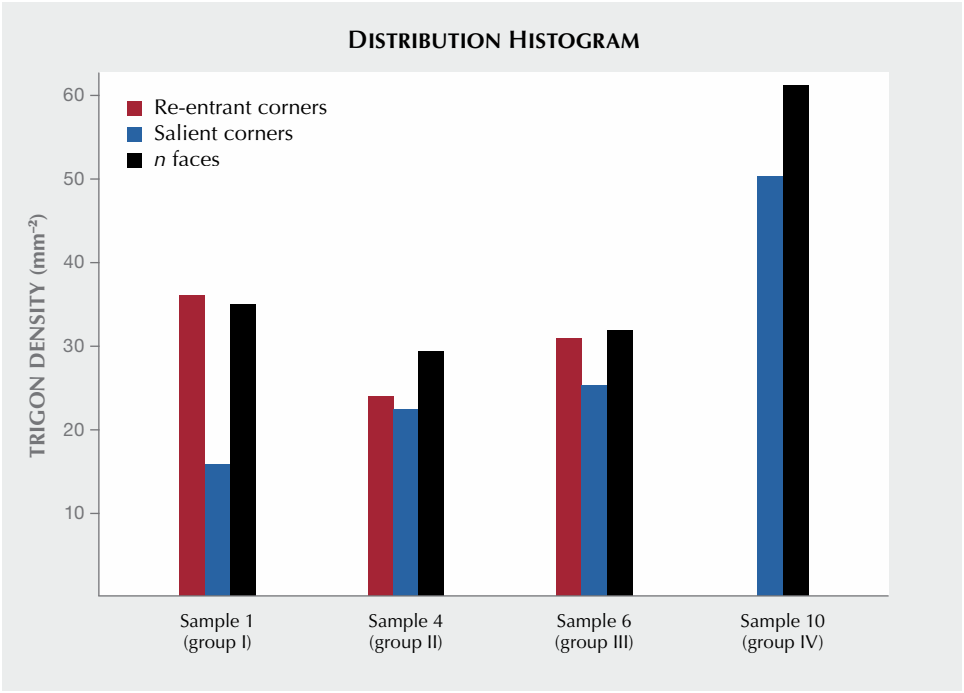

Figure 8. This distribution histogram shows the density (number/mm^2) of trigons found on faces n *and* n* *in re-entrant corners and in salient corners of samples 1, 4, 6, and 10 from morphology groups I, II, III, and IV, respectively.*

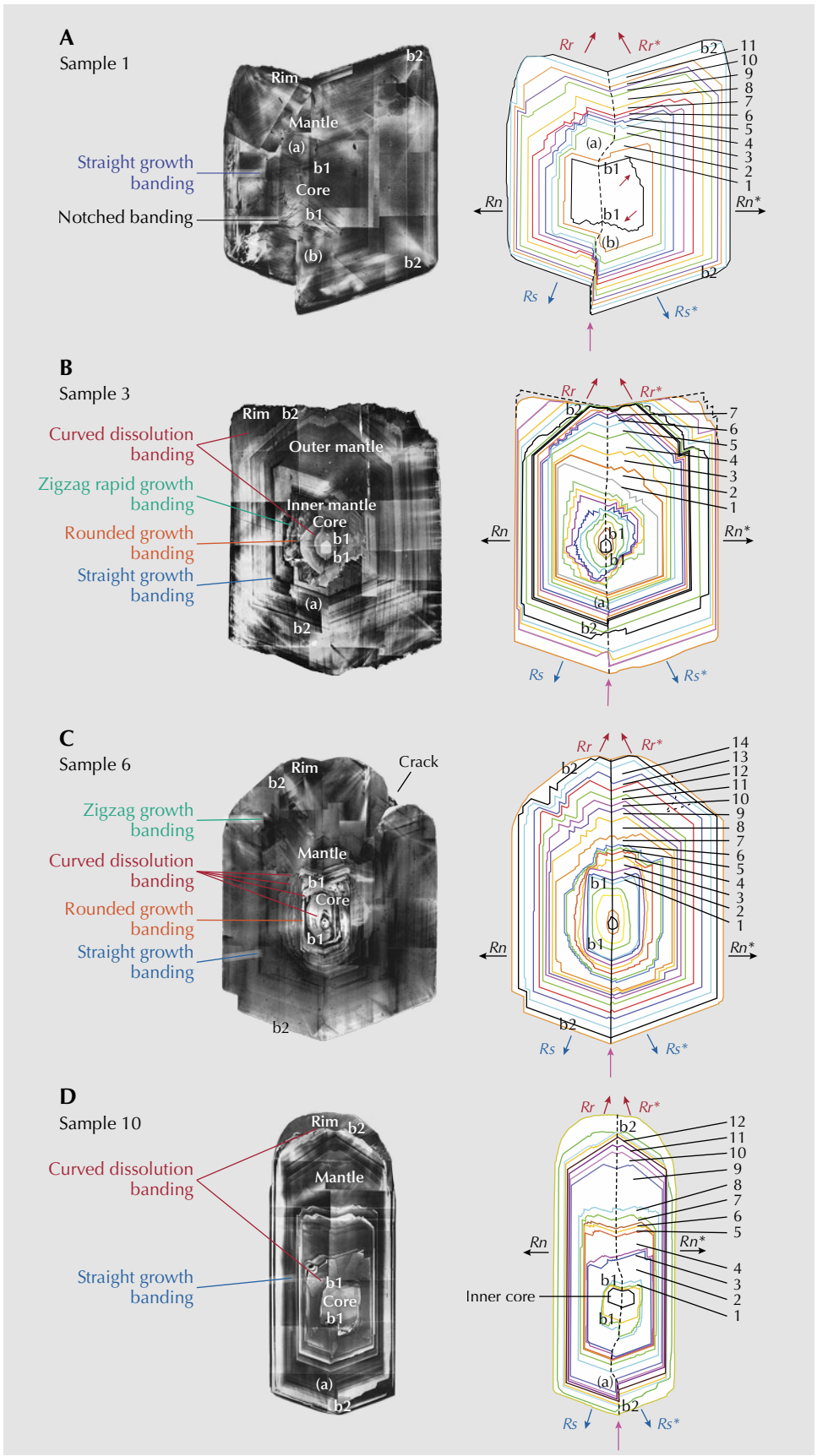

Figure 9. Left: CL images of a plane cutting through the center of samples 1 (A), 3 (B), 6 (C), and 10 (D) reveal a zonal growth structure. The growth stages are divided into three regions, where the growth bands exhibit rounded characteristics that are interrupted by a dissolution process during the growth period. The boundaries are labeled "b1" between the core and mantle and "b2" between the mantle and rim. Right: Illustrations of the growth banding corresponding to the zonal structure. An arrow indicates the direction of the normal growth rate on each face.

According to the CL image of the sliced plane, the crystal displays twinning from its initial growth stage. The entire growth stage can be divided into three zones: core, mantle, and rim, separated by the discordant bands b1 and b2.

In the core zone, a contact twin forms a re-entrant corner with an angle of 141° between the two smooth growth bands of the *r* and *r** {111} faces. However, at the salient corner, the growth bands are marked by zigzag banding (as indicated by the red arrows in figure 9A, right), and some areas of the core may have cracked and broken away during the initial growth stage.

In the mantle zone, the zoning exhibits the typical shape of contact-twinned crystals bounded by {111} faces, creating perfect re-entrant corners. The growth bands of face *r** (as shown in figure 9A, labeled "a" in the illustration) grew larger than those of face *r*, causing the twin boundary to lean to the right. As a result, both faces *r* and *r** became thicker than the other faces, transforming the re-entrant corner from shape i to shape iii. This morphology consists of high-index {hhk} faces with stepped growth layers surrounding a small re-entrant corner at the top, ultimately ending in a thicker, flattened triangular form with the re-entrant corner reverting to shape i. At the salient corner, face *s** (figure 9A, right, labeled "b") grew larger than face *s*, leading to the right crystal being larger and protruding farther than the left. Based on microscopic observations, a significant number of trigons originate at the stacked lamellae growth layers on the *s** surface, indicating preferential spiral growth facilitated by these cooperative screw dislocations on the *s** surface.

In the rim zone (where the border between the mantle and rim is labeled "b2"), the edge of each corner of the {111} face displays a slightly rounded band but develops a perfect concave re-entrant corner resembling shape i. This macle crystal underwent a low degree of dissolution in the final stage.

Sample 3 was sliced into four planes, and the CL image of the center plane is displayed in figure 9B. In the core zone, labeled "b1," the small core shows a high CL intensity, presenting a smooth rounded surface with an apex corner instead of a concave re-entrant corner. This rounded apex corner can be understood as having formed through a dissolution process following the completion of growth on the re-entrant corners during the initial growth stage of this contact-twinned macle crystal. The mantle zone is further divided into two parts; the inner mantle part exhibits a highly complex zonal structure. Several curved growth layers cover the core zone and extend outward in succession. Following this stage, distinct zigzag-shaped step zonings appear, indicating that anti-skeletal faces develop under conditions of high carbon supersaturation. The crystal shows a flattened morphology in the outer mantle with clearly defined straight zoning lines. Faces *r* and *r** in the re-entrant corner grew faster than the other faces (*n* and *n** and *s* and *s**), resulting in the transformation of the re-entrant corner from shape i to shape iv and the formation of a perfect apex corner bounded by {111} faces during the growth stage. In the salient corner, faces *s* and *s** grew in competition, with face *s* (figure 9B, labeled "a") growing larger than face *s** and protruding slightly. A dissolution texture was again noted between the outer mantle and rim (labeled "b2"). In the rim zone, the crystal gradually formed a re-entrant corner once more, covered by several zonings of the {111} face under relatively high carbon supersaturation conditions. In the salient corner, face *s** grew larger, ultimately becoming equal to the growth layer of face *s*. The protrusion of the growth bands did not occur in the final growth stage.

Sample 6 was sliced into three planes, and the CL image of the central plane of the crystal is shown in figure 9C. The core zone displays several rounded growth band morphologies, with the curved surfaces resulting from multiple dissolution processes during the early stages of crystallization. The crystal began twinning from the initial growth stage, with the twin boundary running through the center of all zones. In the mantle, thin stepped lamellae growth layers developed on the curved {111} faces and transitioned from a rounded shape to a flattened morphology with a re-entrant corner. Subsequently, faces *r* and *r** at the re-entrant corners grew faster than the other faces, transforming the re-entrant corner into an apex corner, which was nearly covered by zigzag and stepped {111} *r** faces, along with a very smooth {111} *r* face. However, a small concave re-entrant corner remains at the top until the latest growth stage. Faces *s* and *s** grew almost equally on the salient corner side. In the rim zone, each corner displays a slightly rounded habit, but the plane surface of each {111} face shows no curved structure, indicating that this macle crystal underwent a low degree of dissolution. A crack was observed on the right side of the crystal.

Sample 10 was sliced and polished multiple times into six planes. The CL image of the central plane and a schematic drawing are shown in figure 9D. The core zone displays a bright CL image, with the inner

part characterized by a morphology defined by smooth {111} faces featuring a re-entrant corner (red arrows). In the mantle zone, the crystal exhibits the most flattened morphology with distinct growth bands. Faces *r* and *r** in the re-entrant corner developed more rapidly than the other faces, gradually transforming the re-entrant corner from shape i to shape iv. On the salient corner side, faces *s* and *s** grew in competition, with the growth layers of face *s** in the right domain developing faster and larger than those in the left, causing a shift of the twin plane to the left side and an outward protrusion of the growth bands. During the later growth stage of the mantle zone, preferential growth occurred at face *s*, which developed faster and larger than face *s**. As a result, the twin boundary tilted to the right side. The twin boundary plane that spans the entire crystal is not straight but features a downwardly curved twin plane. In the rim zone is a very flattened and elongated twin crystal with a slightly rounded apex corner, bounded by curved {111} faces that have been somewhat altered by dissolution action. Comparing the four crystals from the four groups, sample 10 is significantly flatter than the other crystals.

Morphological Variation. Because the core and rim exhibit a complex zonal structure that prevents reliable data acquisition, only four samples' mantle zones were studied in detail. The width of growth banding from each face in the mantle zone was measured using the CL image, and the value was adjusted according to the actual size of sample 1 (table 1). The ratios *Rr*/*Rn* (the growth rate of face *r* versus the growth rate of face *n*) and *Rs*/*Rn* (the growth rate of face *s* versus the growth rate of face *n*) of the mantle zone in each twin were estimated by measuring the growth band widths (box B).

The growth rate ratio data (*Rr*/*Rn* and *Rs*/*Rn*) were collected from growth bands 1 to 11 in the mantle zone of sample 1 and are plotted in figure 10A. A small red circle marks the left side of the macle crystal, while a blue circle represents the right side. The arrow's direction indicates the plot sequence from bands 1 to 11.

Most of the data is plotted within the range between *Rr*/*Rs* = 1 and 2. The ratios display a slightly different trend in both single crystals. The ratios (*Rr*/*Rn* and *Rs*/*Rn*) gradually increase to the area where *Rr*/*Rs* > 1 from the initial data plot, indicating that the preferential growth at the re-entrant corner is slightly faster than the growth at the salient corner, resulting in a large re-entrant corner. Then both ratios decrease to a level close to the lower range of *Rr*/*Rn* < 0.5 and *Rs*/*Rn* < 0.5. The last few plotted points show that the ratios increase briefly and then stabilize near the region where *Rr*/*Rn* = 1 and *Rs*/*Rn* = 1.

TABLE 1. Width of growth banding (in μm) from each face in the mantle zone from sample 1.

	r	*r**	*n*	*n**	*s*	*s**	*Rr*/*Rn*	*Rr**/*Rn**	*Rs*/*Rn*	*Rs**/*Rn**
Band 1	43.15	69.58	49.65	88.95	41.47	79.02	0.8690	0.7822	0.8352	0.8883
Band 2	215.60	94.48	57.13	74.27	61.75	78.74	4.4039	1.2721	1.0807	1.0602
Band 3	57.06	93.22	41.96	38.39	34.97	57.13	1.3600	2.4281	0.8333	1.4881
Band 4	31.61	45.17	35.31	57.76	24.27	34.06	0.8950	0.7821	0.6871	0.5896
Band 5	22.45	37.34	30.91	108.50	27.97	32.59	0.7262	0.4430	0.9050	0.3004
Band 6	29.93	29.93	35.03	63.57	34.97	31.40	0.8543	0.4708	0.9980	0.4939
Band 7	64.62	64.62	39.44	90.14	44.41	47.62	1.6383	0.7168	1.1259	0.5283
Band 8	87.55	102.70	50.63	92.24	76.43	62.24	1.7293	1.1130	1.5096	0.6747
Band 9	50.84	50.84	30.56	48.25	32.66	48.25	1.6636	1.0536	1.0686	1.0000
Band 10	34.69	34.69	38.32	35.59	31.82	35.80	0.9051	0.9745	0.8303	1.0059
Band 11	40.83	40.87	31.54	32.03	36.36	36.22	1.2945	1.2759	1.1530	1.1310

Box B: Estimation of Growth Rate Ratio by Measuring the Growth Band

A natural crystal is bound by a set of flat faces that relate to one another through symmetry. The forms that crystals take result from the conditions under which they grow. The same crystal may exhibit different morphologies depending on the growth rates in different crystallographic directions throughout the growth process (figure B-1). Fluctuations in growth rates are recorded as variations in perfection and homogeneity, such as growth sectors and growth banding. Additionally, the ratio of growth rates at any given time cannot be directly estimated from the crystal's external form. Therefore, linear growth rates can be inferred by measuring the widths of growth bands that appear as alternating light and dark bands in the zonal structure of the crystal using this simplified model:

$$\textit{width of growth band} = [\textit{growth rate}] \times [\textit{time}] \qquad \text{(B-1)}$$

The growth rate ratio from different growth faces that belong to the same isochronous face can be expressed as follows, where $R1$ = growth rate 1 and $R2$ = growth rate 2:

$$\frac{\textit{width of growth band 1}}{\textit{width of growth band 2}} = \frac{(R1) \times \textit{time}}{(R2) \times \textit{time}} = (R1/R2) \qquad \text{(B-2)}$$

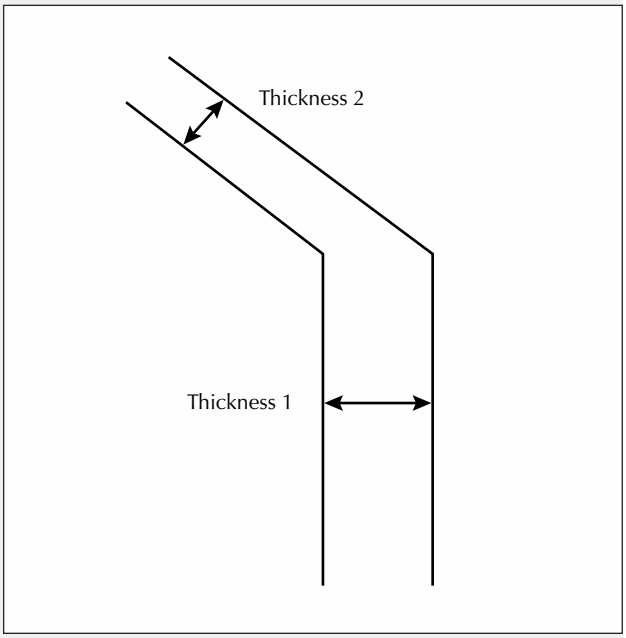

Figure B-1. Illustration of two growth bands showing varying thicknesses on different surfaces belonging to one growth phase.

In sample 3, the core, inner mantle, and rim zones display curved dissolution banding and a complex zigzag zonal structure, enabling the measurement of growth band widths from 1 to 7 in the outer mantle area. The ratios from bands 1 to 5 were plotted within the field of $Rr/Rs > 2$, while the ratios of bands 6 and 7 were plotted in the range between $Rr/Rs = 2$ and $Rr/Rs = 1$ in figure 10B. The left side of the macle crystal is marked with a red circle, while the right is labeled with a blue circle. The ratios for both sides of the twin exhibit a similar trend. The ratios (Rr/Rn and $Rr^{\star}/Rn^{\star}$) initially rise significantly to the range where $Rr \geqq 2Rs$, where the growth rates (Rr and $Rr^{\star}$) at the re-entrant corner are prominent, causing the re-entrant corner to transform into an apex corner, which is bounded only by {111} faces during the growth process.

The ratios then decrease repeatedly to the lower range of $Rr/Rs < 2$, where the effects at both the re-entrant and salient corners were not anticipated. These trends suggest that carbon supersaturation diminished at the beginning of crystal growth in the initial stage of this outer mantle zone, with the re-entrant corner effect playing a significant role in forming an apex corner and shaping the twin into a flattened form. During the latter half of the growth stage of the mantle zone, carbon supersaturation increased significantly, leading to growth on every face of the crystal, with two-dimensional nucleation preferentially occurring near the crystal's edges to create a large surface of *n*, *s*, and *r*, thus recreating a re-entrant corner similar to shape ii.

Figure 10C plots the 14 data points of band width from bands 1 to 14 in the mantle zone of sample 6. Most data points are plotted in the range where $Rr/Rn > 1$ and $Rs/Rn > 1$. The ratios in both sides of the twin show a consistent trend. The ratios first increase to the range where $Rr > 2Rs$, indicating a tendency for the re-entrant corner to transition into an apex corner due to preferential growth at the re-entrant corner under relatively low carbon supersaturation conditions. Simultaneously, the ratio of Rs/Rn also shows a high value of 1.6, suggesting that the preferential growth at the salient corner is expected to produce a unidirectionally flattened shape. Subsequently, both ratios (Rr/Rn and Rs/Rn) decline rapidly to the range where $Rr/Rn < 1$ and $Rs/Rn < 1$ from bands 3 to 5, where the effects of the re-entrant and salient corners were not anticipated. The ratios from bands 6 to 8 display a similar pattern,

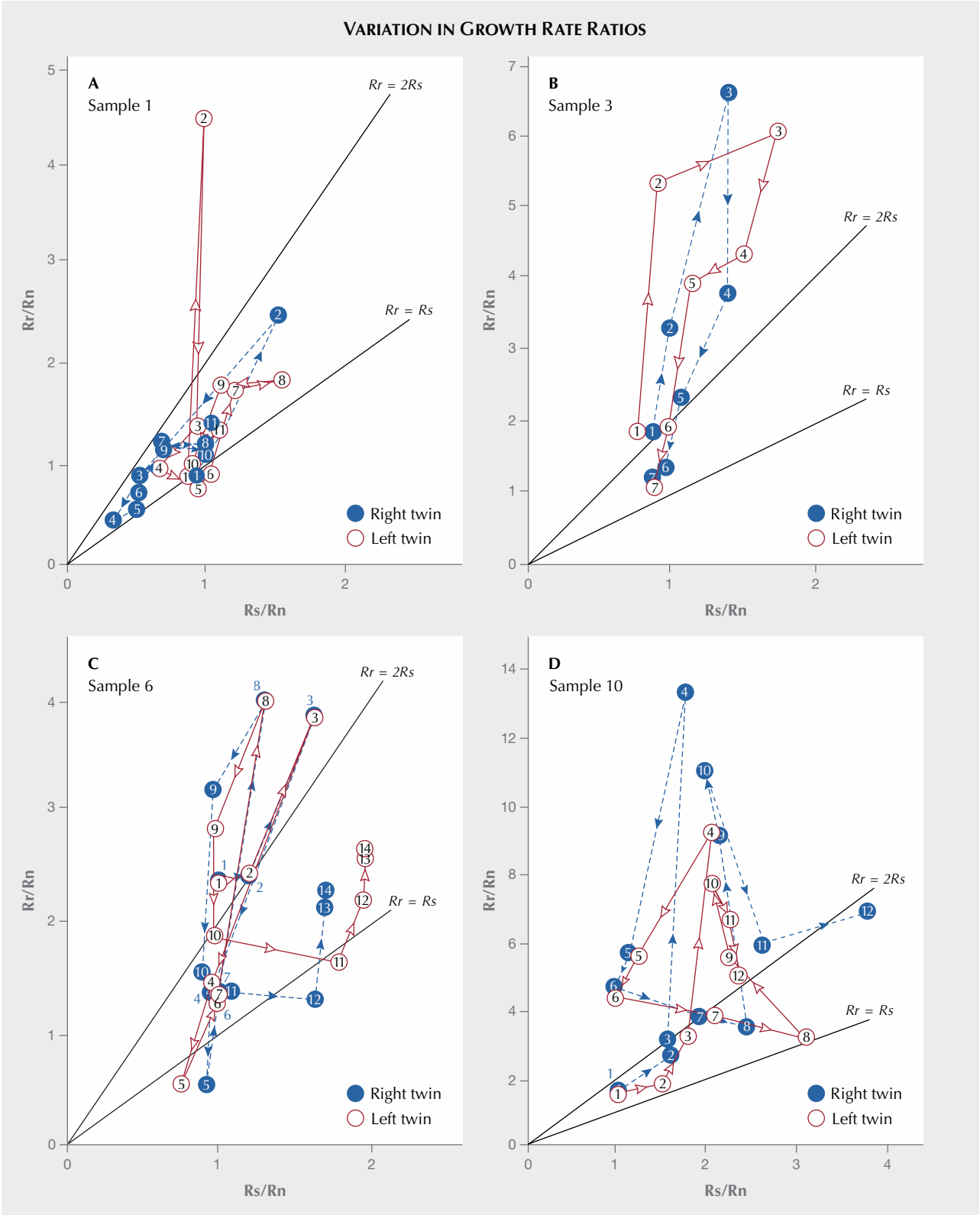

Figure 10. The ratios Rr/Rn *and* Rs/Rn*, indicated by red circles, are calculated based on the growth banding observed in the left twin of samples 1, 3, 6, and 10. Meanwhile, the growth rate ratios* Rr*/Rn* *and* Rs*/Rn*, represented by solid blue circles, are derived from the growth banding in the right twin. The lines for* Rr = Rs *(or* Rr/Rs = *1) and* Rr = 2Rs *(or* Rr/Rs = *2) are also displayed.*

increasing again to the range of $Rr > 2Rs$ and reaching a peak value of $Rr/Rn = 4$, resulting in the re-entrant corner becoming almost concealed by stacking growth layers on the {111} faces over time. However, the ratios from bands 9 to 10 quickly decreased to the range between $Rr/Rs = 1$ and 2, and the ratios (Rs/Rn) from bands 11 and 12 for both twins showed a significant change from values of unity (1) to 1.97 and 1.63, respectively, dropping below the $Rr < Rs$ line, where preferential growth on the salient corner became dominant, forming thick growth banding that enhanced the flatness of the twin. In the final stage of the mantle zone, the ratios Rr/Rn and Rs/Rn from bands 13 and 14 increased again.

The data for the Rr/Rn and Rs/Rn ratios from bands 1 to 12 in the mantle zone of sample 10 are plotted in figure 10D. Most of the data fall within the range where $Rr/Rn > 1$ and $Rs/Rn > 1$. The ratios from bands 1 to 4 initially increased to the range of $Rr \geqq 2Rs$, with anticipated effects from both the re-entrant and salient corners. The ratio of Rr/Rn reaches its peak of 13, marking the transition from the re-entrant corner to the apex corner. Conversely, the expected preferential growth at the salient corner led to face s^* growing thicker and larger than face s, causing the twin boundary to shift to the left side. Subsequently, both ratios decreased to Rr/Rn of 4.3 and Rs/Rn of 1. At this juncture, the preferential growth at the re-entrant corner gradually weakened, while the growth at the salient corner was entirely unexpected. Following this growth stage, the ratio of Rs/Rn (from bands 7 to 8) shows a significant rise, and the anticipated preferential growth at the salient corner is expected to create thick growth bands (layers) on faces s and s^*. Consequently, the morphology of this macle crystal is noticeably flatter than that of macle crystals from other groups. In the final stage of the mantle zone, the Rr/Rn ratio (bands 9 to 10) increased again. The {111} face completely covers the re-entrant corner, showcasing a perfect apex corner and corresponding to the shape iv form of a re-entrant corner. However, the Rr/Rn ratio (bands 11 to 10) decreased rapidly, while the Rs/Rn ratio continued to trend upward, indicating a preference for growth at the salient corner, forming a highly elongated macle crystal.

DISCUSSION

Establishing a Model of Morphological Variation for Contact Twins. When a twinned crystal forms in its initial stage and the normal growth rates of the r, s, and n faces—designated Rr, Rs, and Rn—remain consistent throughout the growth process, a morphological variation model is geometrically represented by two ratios: Rr/Rn and Rs/Rn (figure 11). When all octahedral faces exhibit identical growth rates ($Rr/Rn = 1$, $Rs/Rn = 1$; see figure 11), the morphology features both re-entrant and salient corners, appearing flatter than those formed by two regular octahedra ($Rr/Rn = 0.5$, $Rs/Rn = 0.75$; see figure 12).

An increase in the ratios Rr/Rn or Rs/Rn indicates preferential growth at re-entrant corners or salient corners, respectively. A rise in both ratios leads to a flatter morphology. Previous studies have not explored preferential growth at salient corners (Rs/Rn) in contact-twinned macle diamonds (Becke, 1911; Chudoba, 1927; Stranski, 1949; Hartman, 1956, Sunagawa, 1975; Sunagawa et al., 1979; Sunagawa and Yasuda, 1983; Sunagawa and Lu, 1987). In the range where $Rr \geq 2Rs$, re-entrant corners disappear and transform into apexes covered by neighboring s and s^* faces. In this case, morphology is influenced solely by the ratio of Rs/Rn. When Rr is less than $2Rs$, re-entrant corners begin to appear. The overall shape can display various morphologies depending on the ratio of Rr/Rs. These include shapes with small re-entrant corners at the apexes, well-developed re-entrant corners, and re-entrant corners formed by trapezoidal faces. When $Rr = Rs$ ($Rr/Rs = 1$), the formation of re-entrant corners and salient corners is equal.

Relationship Between the Ratio of Growth Rate and External Morphology. We proposed the following equations to connect the growth rate ratio with the flatness of the external morphology of the macle crystals:

$$\frac{Rr}{Rn} = \frac{4}{3}\frac{h}{d}\sin\theta - \cos\theta + \frac{2l}{d}\sin\alpha \quad (1)$$

$$\frac{Rs}{Rn} = \frac{2}{3}\frac{h}{d}\sin\theta + \cos\theta + \frac{2l}{d}\sin\alpha \quad (2)$$

where h is the height of face n, d is the thickness of the crystal, l is the length of the edge at the re-entrant corner, θ is the interfacial angle between face n and face r, and α is the interfacial angle between the edge of the re-entrant corner and face n (again, see these flatness indicators in box A, figure A-1). The ratios Rr/Rn and Rs/Rn of the 10 studied crystals from the four morphology groups were estimated based on the flatness of their external morphology. They are plotted in figure 12 and labeled with diamond markers in different colors for each group of crystals.

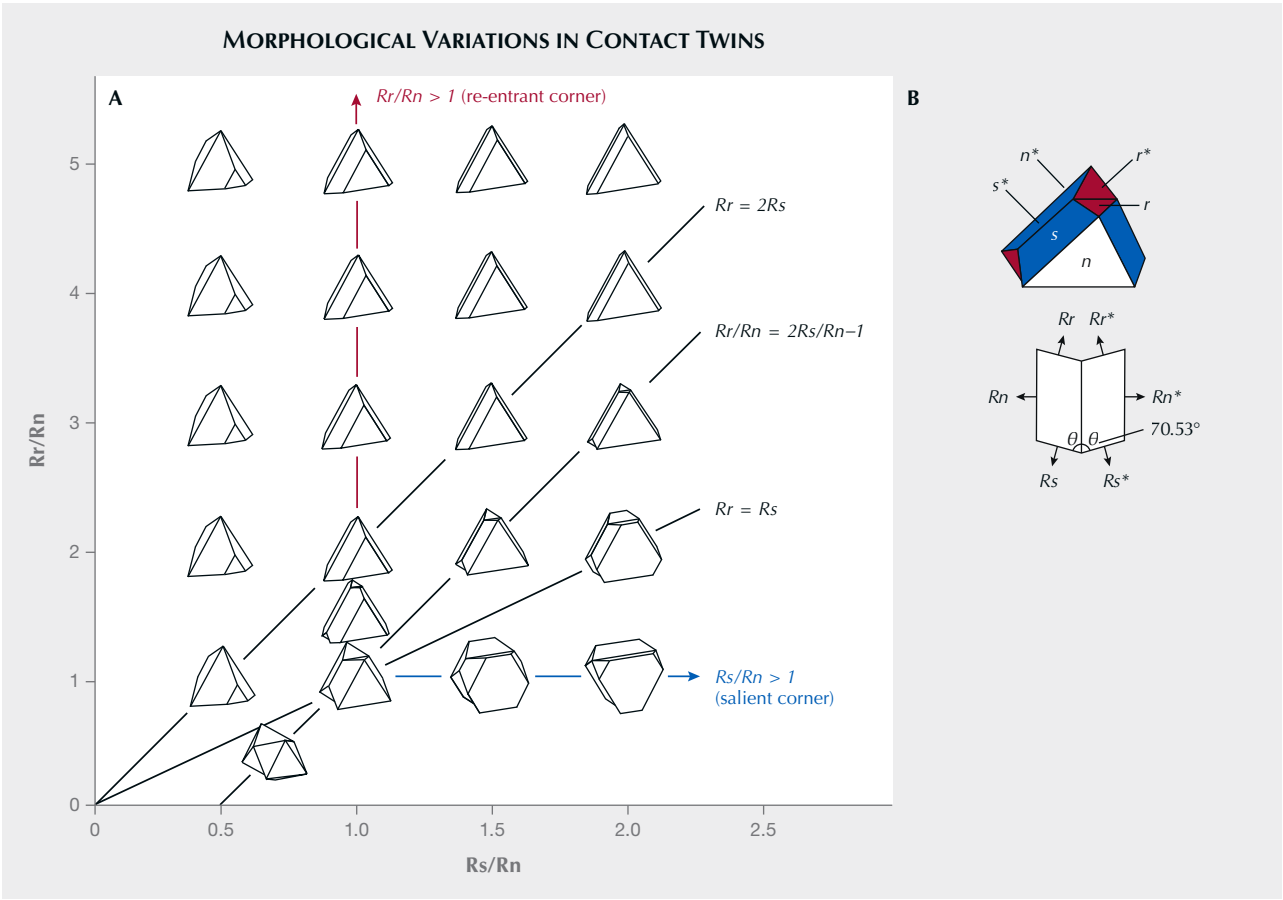

Figure 11. A: Schematic illustration of the model of morphological variations in contact twins caused by changes in the ratios Rr/Rn *and* Rs/Rn. *The lines for* Rr = Rs *(or* Rr/Rs = *1),* Rr = 2Rs *(or* Rr/Rs = *2), and* Rr/Rn = 2Rs/Rn–1 *are also shown. The re-entrant effect is expected if* Rr/Rn > *1. Additionally, if* Rs/Rn *exceeds 1, the salient corner effect can be anticipated. B: Illustration of a contact twin. Three types of {111} faces (*r *and* r*, s *and* s*, *and* n *and* n**) along with the normal growth rate of each face (left side of twin:* Rr, Rn, Rs*; right side of twin:* Rr*, Rn*, Rs**) are labeled.*

The macle crystals with shape i and shape ii re-entrant corners show morphologies indicating minimal or no preferential growth at re-entrant and salient corners, with growth morphologies expected to form within the $1 \leq Rr/Rs < 2$ range. Morphology groups III and IV are plotted close to or within the range of line *Rr = 2Rs*. The morphologies of the contact twins feature apex corners but may or may not have re-entrant corners. This aligns with the expectation that preferential growth occurs at both re-entrant and salient corners. The apex corners of morphology group IV discussed here are not covered by flat {111} faces but by high-index {hhk} stepped lamellae faces instead (again, see figure 4, H–J). Group III crystals, characterized by small re-entrant corners, clearly show the stacking of thick growth layers formed at the twin boundary (again, see figure 4, E–G). This suggests that the formation of the high-index faces likely occurs under conditions similar to those required for apex formation by neighboring {111} faces. However, the stacking of these growth layers may result from impurity trapping. Samples 9 and 10 exhibit slightly curved apex corners and underwent low levels of dissolution after completing their growth.

As observed in figure 12, the preferential growth at salient corners does not dominate the growth at re-entrant corners. Nevertheless, it clearly influences the growth of morphology. Two main effects can be considered in this context. The first effect relates to the diffusion fields surrounding the crystals. Salient corners protrude more than the *n* and *n** faces, resulting in higher carbon supersaturation conditions at these corners. Despite this, the preferential growth at salient corners is significantly linked to the re-entrant corner effect, suggesting that the preferential growth of the *s* and *s** faces is primarily controlled by surface kinetics. Therefore, the impact of diffusion fields on

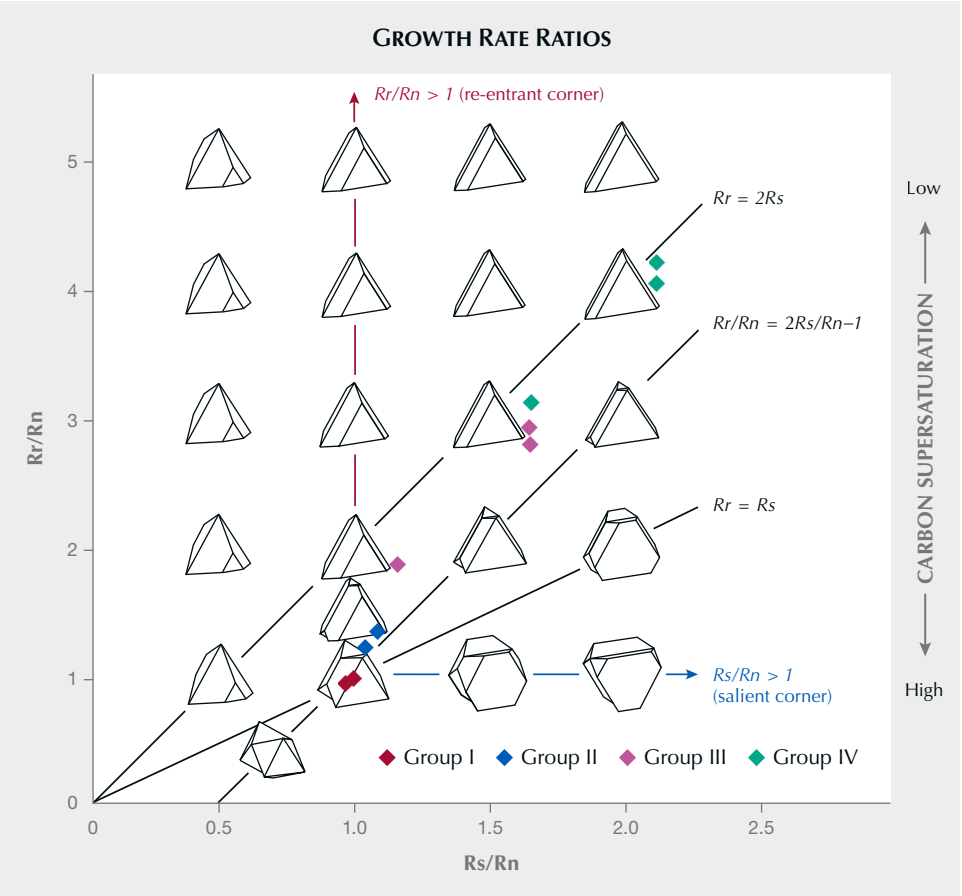

Figure 12. The growth rate ratios of 10 macle crystals from four morphology groups are estimated based on the flatness of their external morphologies. A macle crystal's flatness is strongly related to preferential growth at the re-entrant and salient corners. The relationship between carbon supersaturation and the effects of the re-entrant and salient corners is presented.

preferential growth may be relatively minor. The second effect involves the role of screw dislocations at the twin boundary. When screw dislocations at the twin boundary of salient corners are more abundant than those in the *n* and *n** faces, preferential growth can be expected at the twin boundary, similar to the pseudo re-entrant corner effect (Kitamura et al., 1979). Based on microtopographical surface observations, the surfaces at re-entrant and salient corners in morphology group I and II crystals exhibit predominantly flat growth layers. In contrast, well-defined growth layers extending two-dimensionally outward from the twin boundary of the re-entrant and salient corners were observed in group III and IV crystals. The density and number of trigons at salient corners are more pronounced than in the morphology I and II groups. This indicates that preferential growth at salient corners is primarily driven by screw dislocations generated at the twin boundary. Consequently, groups III and IV exhibit greater morphology flatness than groups I and II.

The Carbon Supersaturation Condition. Under conditions of high carbon supersaturation, growth particles can easily form two-dimensional nuclei across the surface before settling on the most energetically favorable sites. This occurs because the likelihood of growth particles reaching the growing surface significantly increases due to the high carbon supersaturation. Consequently, all sites appear to have a similar capacity to adsorb growth particles, leading to two-dimensional nucleation occurring almost universally on the surface. Considering the Berg effect (Berg, 1938), two-dimensional nucleation is more likely to occur near the crystal's edges. As a result, the re-entrant corner effect is not expected to function at all under conditions of high carbon supersaturation.

Conversely, the normal growth rate of a crystal face is influenced by the number of cooperative screw dislocations. Spiral growth preferentially occurs at energetically favorable sites, but this occurs under low, rather than high, carbon supersaturation conditions (Burton et al., 1949; Hartman, 1956). Thus, the re-entrant and salient corner effects can be anticipated only under relatively low carbon supersaturation conditions. The ratio *Rr*/*Rn* indicates changes in carbon supersaturation during crystal

growth (Kitamura et al., 1979). An increasing value of *Rr*/*Rn* signifies a decrease in carbon supersaturation. In contrast, when *Rr* is less than *Rn*, it indicates increased carbon supersaturation. In this study, the values of *Rr*/*Rn* and *Rs*/*Rn* illustrate the relative differences in growth conditions of four crystals, as shown in figure 13.

It can be inferred that sample 1 formed under conditions of higher carbon supersaturation compared to the other crystals, while sample 10 formed under the lowest carbon supersaturation conditions. Additionally, samples 1 and 3 show a trend of increasing carbon supersaturation during the final stages of growth. Samples 6 and 10 show a decreasing trend in the later stages of growth. As mentioned earlier, we suggest that the carbon supersaturation in the four types of crystals decreased and then increased repeatedly during the growth stage of their mantle zones. In natural crystallization, crystal growth is expected to reduce carbon supersaturation in a closed system, assuming there are no external influences from environmental conditions such as pressure, temperature, or external fluids. Consequently, our data on the varying growth rates indicate that carbon supersaturation does not change in a simple, consistent manner as traditionally believed; rather, it can fluctuate during the growth process. Therefore, introducing additional carbon into the growth environment or significantly changing pressure and temperature conditions may explain the observed increases in carbon supersaturation during certain growth stages of the specimens we studied.

Figure 13. Diagram illustrating the estimated changes in carbon supersaturation during the crystal growth of contact-twinned macle diamonds. It emphasizes the relationship between carbon supersaturation and growth rate (growth band) in the crystal's mantle zones, particularly focusing on the preferential growth effect at the re-entrant corner. Four macle crystals—samples 1 (group I), 3 (group II), 6 (group III), and 10 (group IV)—show distinct fluctuations in carbon supersaturation throughout their growth period. The horizontal axis represents the distance from the first to the last growth banding in the crystal's mantle zone.

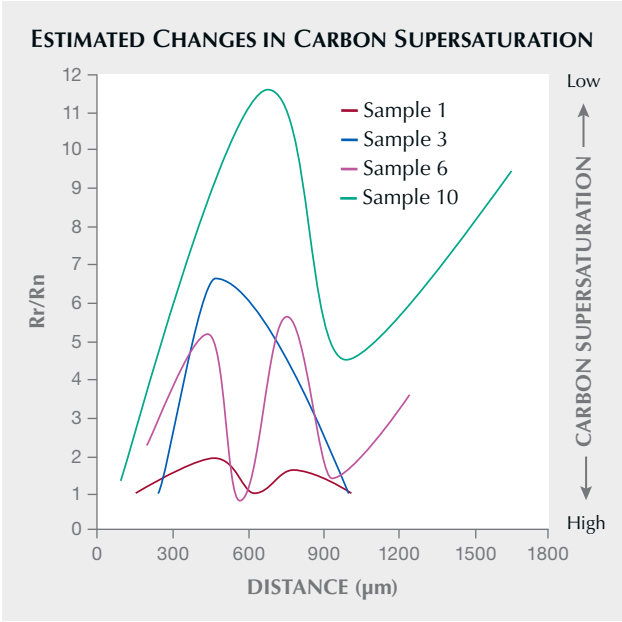

CONCLUSIONS

Based on observations of external morphology, surface microtopography, and internal zonal structure of contact-twinned natural macle diamonds, their re-entrant corners can be classified into four distinct shapes (i, ii, iii, and iv) determined by modifications from growth layers. Morphology groups I and II have been previously identified and are characterized by either very flat {111} surfaces or a few thicker growth layers at the re-entrant corners. However, this study reports morphology groups III and IV (figure 14) for the first time. Groups III and IV are distinguished by the accumulation of thick growth layers at the twin boundaries of the re-entrant corners, leading to the formation of four high-index {hhk} faces surrounding a small re-entrant corner or being completely covered by smooth or stepped {hhk} surfaces, rather than exhibiting a re-entrant corner. The four macle diamond crystal morphology groups are more flattened than a twin formed solely by the contact of two regular octahedra bounded by {111} faces. The effects of re-entrant and salient corners play a significant role in their growth. The macle crystals from groups III and IV are flatter than those from groups I and II. The growth mechanism can be explained by preferential growth occurring not only at the re-entrant corners but also significantly influencing the salient corners of the contact-twinned macle diamonds.

Macle crystals' internal zonal growth structure reveals distinct morphological changes during growth. The zonal structure of four sliced and polished macle crystals indicates that growth begins with a morphology featuring re-entrant corners. Over time, this morphology transforms into one with apex corners that gradually become covered by {111} faces, replacing the re-entrant corners.

Figure 14. A gold pendant adorned with four flattened triangular macle rough diamonds with re-entrant corners belonging to morphology groups III and IV, weighing 0.945 total carats. Photo by Tetsuya Chikayama.

At the end of the growth process, a flattened contact twin may form, which can revert to a morphology with re-entrant corners or result in a very flattened form ending with a smooth or curved apex corner. It should be noted that dissolution can occur during the growth stage and lead to a curved zonal structure of growth banding.

The flatness of the external morphology of macle diamonds is closely linked to the preferential growth occurring at the re-entrant and salient corners. The changes in the morphology of macle diamonds can be interpreted as fluctuations in carbon supersaturation conditions during the crystallization process. By measuring the width of the growth bands in these crystals, we estimated that the growth conditions of macle diamonds fluctuated, indicating that carbon supersaturation levels decreased and increased repeatedly throughout their growth. Large, flattened, thin triangular macle diamonds, characterized by apex corners, are believed to form under relatively lower carbon supersaturation than crystals with a thick triangular morphology featuring concave re-entrant corners.

To our knowledge, this study is the first to provide a comprehensive understanding of the crystal growth of natural macle diamonds, revealing the complex growth processes that occur deep within the earth.

ABOUT THE AUTHORS

Dr. Ahmadjan Abduriyim is president of Tokyo Gem Science and director of GSTV Gemological Laboratory in Tokyo. Dr. Masao Kitamura is emeritus professor of the Division of Earth and Planetary Sciences, Department of Geology and Mineralogy at the Graduate School of Science, Kyoto University, Japan.

ACKNOWLEDGMENTS

The authors would like to sincerely thank Norimasa Shimobayashi of Kyoto University for critically reading the manuscript and for productive discussions, encouragement, and guidance throughout this study. We also greatly appreciate the technical assistance and insightful discussions provided by our former colleagues Junichi Minato, Jun Kawano, and Yusuke Seto in the Department of Geology and Mineralogy at the Graduate School of Science, Kyoto University.

REFERENCES

Abduriyim A., Kitamura M. (2002) Growth morphology and change in growth conditions of a spinel-twinned natural diamond. *Journal of Crystal Growth*, Vol. 237–239, pp. 1286–1290, http://dx.doi.org/10.1016/S0022-0248(01)02146-7

Battaile C.C., Srolovitz D.J., Butler J.E. (1998) Atomic-scale simulations of chemical vapor deposition on flat and vicinal diamond substrates. *Journal of Crystal Growth*, Vol. 194, No. 3-4, pp. 353–368, http://dx.doi.org/10.1016/S0022-0248(98)00685-X

Becke F. (1911) Über die ausbildung der zwillingskristalle. *Fortschritte der Mineralogie, Kristallographi und Petrographie*, Vol. 1, pp. 48–65.

Berg W.F. (1938) Crystal growth from solutions. *Proceedings of the Royal Society A*, Vol. 164, No. 916, pp. 79–95, http://dx.doi.org/10.1098/rspa.1938.0006

Burton W.K., Cabrera N., Frank F.C. (1949) Role of dislocations in crystal growth. *Nature*, Vol. 163, pp. 398–399.

Butler J.E., Oleynik I. (2008) A mechanism for crystal twinning in the growth of diamond by chemical vapour deposition. *Philosophical Transactions of the Royal Society A*, Vol. 366, No. 1863, pp. 295–311, http://dx.doi.org/10.1098/rsta.2007.2152

Chudoba K. (1927) Zwillingspersistenzen. *Zeitschrift für Kristallographie*, Vol. 65, pp. 225–237.

Frank F.C., Puttick K.E., Wilks E.M. (1958) Etch pits and trigons on diamond: 1. *Philosophical Magazine*, Vol. 3, No. 35, pp. 1262–1272, http://dx.doi.org/10.1080/14786435808233308

Harris J.W., Hawthorne J.B., Oosterveld M.M., Wehmeyer E. (1975) A classification scheme for diamond and a comparative study of South African diamond characteristics. *Physics and Chemistry of the Earth*, Vol. 9, pp. 765–783, http://dx.doi.org/10.1016/B978-0-08-018017-5.50053-5

Hartman P. (1956) On the morphology of growth twins. *Zeitschrift für Kristallographie – Crystalline Materials*, Vol. 107, No. 1-6, pp. 225–237, http://dx.doi.org/10.1524/zkri.1956.107.16.225

Hirabayashi K., Kimura T., Hirose Y. (1993) Morphology of flattened diamond crystals synthesized by the oxy-acetylene flame method. *Applied Physics Letters*, Vol. 62, pp. 354–356, http://dx.doi.org/10.1063/1.108955

Kitamura M. (1990) Growth history of spinel-twinned diamond. *Proceedings of the Third Topical Meeting on Crystal Growth Mechanism* (Tokyo), pp. 95–98.

Kitamura M., Hosoya S., Sunagawa I. (1979) Re-investigation of the re-entrant corner effect in twinned crystals. *Journal of Crystal Growth*, Vol. 47, No. 1, pp. 93–99, http://dx.doi.org/10.1016/0022-0248(79)90162-3

Kitamura M., Fudaki M., Shwin K., Shimobayashi N. (1992) A cathodoluminescence microscope and its application to the study of growth zoning of minerals. *Mineralogical Journal*, Vol. 16, No. 2, pp. 108–116, http://dx.doi.org/10.2465/minerj.16.108

Lang A.R. (1964) Dislocations in diamond and the origin of trigones. *Proceedings of the Royal Society of London A*, Vol. 278, No. 1373, pp. 234–242, http://dx.doi.org/10.1098/rspa.1964.0057

Ming N.-B., Sunagawa I. (1988) Twin lamellae as possible self-perpetuating step sources. *Journal of Crystal Growth*, Vol. 87, No. 1, pp. 13–17, http://dx.doi.org/10.1016/0022-0248(88)90339-9

Orlov Y.L. (1977) *The Mineralogy of the Diamond*. John Wiley & Sons, New York.

Ponahlo J. (1992) Cathodoluminescence (CL) and CL spectra of De Beers experimental synthetic diamonds. *Journal of Gemmology*, Vol. 23, No. 1, pp. 3–18.

Sinkankas J. (1964) *Mineralogy for Amateurs*. Van Nostrand Reinhold Company, Princeton, New Jersey, pp. 96–105.

Stranski L.N. (1949) General discussion. *Discussions of the Faraday Society*. No. 5, pp. 66–69.

Sunagawa I. (1975) Mechanism of formation of growth twins, and their macro- and micro-morphology. *Journal of the Mineralogical Society of Japan*, Vol. 12, No. 2, pp. 117–131, http://dx.doi.org/10.2465/gkk1952.12.117 [in Japanese]

Sunagawa I., Takahashi J., Aonuma K., Takahashi M. (1979) Growth of quartz crystals twinned after Japan law. *Physics and Chemistry of Minerals*, Vol. 5, pp. 53–63, http://dx.doi.org/10.1007/BF00308168

Sunagawa I., Yasuda T. (1983) Apparent re-entrant corner effect upon the morphologies of twinned crystals; A case study of quartz twinned according to Japanese twin law. *Journal of Crystal Growth*, Vol. 65, No. 1-3, pp. 43–49, http://dx.doi.org/10.1016/0022-0248(83)90034-9

Sunagawa I., Tsukamoto K., Yasuda T. (1984) Surface microtopographic and X-ray topographic study of octahedral crystals of natural diamond from Siberia. In I. Sunagawa, Ed., *Materials Science of the Earth's Interior*. Terra Scientific Publishing, Tokyo, and Reidel, Boston, pp. 331–349.

Sunagawa I., Lu T. (1987) Apparent re-entrant corner effect due to impurities in ribbon-like morphology of hematite twins. *Mineralogical Journal*, Vol. 13, No. 6, pp. 328–346, http://dx.doi.org/10.2465/minerj.13.328

Tappert R., Tappert M.C. (2011) *Diamonds in Nature: A Guide to Rough Diamonds*. Springer-Verlag, Berlin, pp. 15–42.

Yacoot A., Moore M., Machado W.G. (1998) Twinning in natural diamond. I. Contact twins. *Journal of Applied Crystallography*, Vol. 31, pp. 767–776, http://dx.doi.org/10.1107/S0021889898005317